blood®
Regular Article

LYMPHOID NEOPLASIA

13q12.2 deletions in acute lymphoblastic leukemia lead to upregulation of *FLT3* through enhancer hijacking

Minjun Yang,[1] Setareh Safavi,[1] Eleanor L. Woodward,[1] Nicolas Duployez,[2,3] Linda Olsson-Arvidsson,[1,4] Jonas Ungerbäck,[5] Mikael Sigvardsson,[5,6] Marketa Zaliova,[7,8] Jan Zuna,[7,8] Thoas Fioretos,[1,4] Bertil Johansson,[1,4] Karolin H. Nord,[1] and Kajsa Paulsson[1]

[1]Division of Clinical Genetics, Department of Laboratory Medicine, Lund University, Lund, Sweden; [2]Laboratory of Hematology, Centre Hospitalier Universitaire (CHU) Lille, Lille, France; [3]Unité Mixte de Recherche en Santé (UMR_S) 1172, INSERM/University of Lille, Lille, France; [4]Division of Laboratory Medicine, Department of Clinical Genetics and Pathology, Skåne University Hospital, Lund, Sweden; [5]Division of Molecular Hematology, Lund Stem Cell Center, Department of Laboratory Medicine, Lund University, Lund, Sweden; [6]Department of Clinical and Experimental Medicine, Linköping University, Linköping, Sweden; [7]Department of Pediatric Hematology and Oncology, Second Faculty of Medicine, Charles University/University Hospital Motol, Prague, Czech Republic; and [8]Childhood Leukaemia Investigation Prague (CLIP), Prague, Czech Republic

KEY POINTS

- **Recurrent somatic 13q12.2 deletions in ALL lead to upregulation of *FLT3* through chromatin remodeling and enhancer hijacking.**

Mutations in the FMS-like tyrosine kinase 3 (*FLT3*) gene in 13q12.2 are among the most common driver events in acute leukemia, leading to increased cell proliferation and survival through activation of the phosphatidylinositol 3-kinase/AKT-, RAS/MAPK-, and STAT5-signaling pathways. In this study, we examine the pathogenetic impact of somatic hemizygous 13q12.2 microdeletions in B-cell precursor (BCP) acute lymphoblastic leukemia (ALL) using 5 different patient cohorts (in total including 1418 cases). The 13q12.2 deletions occur immediately 5′ of *FLT3* and involve the *PAN3* locus. By detailed analysis of the 13q12.2 segment, we show that the deletions lead to loss of a topologically associating domain border and an enhancer of *FLT3*. This results in increased *cis* interactions between the *FLT3* promoter and another enhancer located distally to the deletion breakpoints, with subsequent allele-specific upregulation of *FLT3* expression, expected to lead to ligand-independent activation of the receptor and downstream signaling. The 13q12.2 deletions are highly enriched in the high-hyperdiploid BCP ALL subtype (frequency 3.9% vs 0.5% in other BCP ALL) and in cases that subsequently relapsed. Taken together, our study describes a novel mechanism of *FLT3* involvement in leukemogenesis by upregulation via chromatin remodeling and enhancer hijacking. These data further emphasize the role of *FLT3* as a driver gene in BCP ALL. (*Blood*. 2020;136(8):946-956)

Introduction

FLT3, encoding the FMS-like tyrosine kinase 3 (FLT3), is one of the most commonly mutated genes in acute leukemia, with ~30% of acute myeloid leukemia (AML) and ~5% of pediatric B-cell precursor (BCP) acute lymphoblastic leukemia (ALL) displaying mutations.[1] FLT3 is a class III receptor tyrosine kinase that is primarily expressed in the bone marrow, in particular on $CD34^+$ hematopoietic stem and early progenitor cells.[1] Upon binding of the FL ligand, FLT3 dimerizes and tyrosine residues in the tyrosine kinase domains become autophosphorylated. This results in downstream activation of the phosphatidylinositol 3-kinase/AKT-, RAS/MAPK-, and STAT5-signaling pathways and, subsequently, in increased proliferation and reduced apoptosis.[1] The majority of mutations are either internal tandem duplications (ITDs) of the juxtamembrane domain, most common in AML, or activating tyrosine kinase domain mutations, both of which lead to constitutive activation of the FLT3 receptor. Furthermore, high *FLT3* expression is seen in some leukemic subtypes regardless of mutational status, for example, in ALL with high hyperdiploidy (51-67 chromosomes).[2,3]

We have previously reported recurrent somatic hemizygous 13q12.2 microdeletions in childhood BCP ALL, with currently unknown effects.[4,5] The only gene in the deleted region is *PAN3*, which encodes the regulatory subunit of the poly(A)-nuclease (PAN) deadenylation complex (PAN2-PAN3 complex). PAN3 has not previously been implicated in cancer apart from in a single case of myelodysplastic syndrome with a *PAN3/PSMA2* fusion.[6] However, the 13q12.2 deletions are also located immediately 5′ of *FLT3* and we therefore hypothesized that they may affect its expression. Indeed, here we show that 13q12.2 deletions in ALL lead to upregulation of *FLT3* expression by inducing *cis* interactions between the *FLT3* promoter and an enhancer element located distally to the deleted region. Our study thus reveals a novel mechanism of *FLT3* involvement in leukemogenesis.

Patients and methods

Patient cohorts

A total of 1418 BCP ALL cases from 5 different patient cohorts were included in the investigation (supplemental Figure 1, available on the *Blood* Web site). The Lund discovery cohort

(cohort 1) is an expansion of a previously published series consisting of 276 cases genotyped by Illumina BeadChips (Illumina, San Diego, CA) or CytoScan HD single-nucleotide polymorphism (SNP) arrays (Affymetrix/Thermo Fisher Scientific, Waltham, MA).[7] The Therapeutically Applicable Research to Generate Effective Treatments (TARGET) program (https://portal.gdc.cancer.gov/projects; dbGAP accession number phs000464) ALL phase 2 discovery cohort (cohort 2) comprises 783 cases genotyped by the Affymetrix Genome-Wide Human SNP Array 6.0. Three validation cohorts, including high-hyperdiploid ALL cases only, were also included: cohort 3 (n = 123)[8] genotyped by Affymetrix CytoScan HD array; cohort 4 (n = 97)[9] genotyped by Illumina BeadChips; and cohort 5, the TARGET ALL phase 2 validation cohort (n = 139), genotyped by whole-exome sequencing (WES). Informed consent was obtained according to the Declaration of Helsinki and the study was approved by the Ethics Committee of Lund University.

SNP array data analysis

Illumina (.idat files) and Affymetrix (.CEL files) intensity files were analyzed by GenomeStudio v2011.1 (Illumina) and PennCNV (1.0.5),[10] respectively. Copy-number alterations (CNAs) were called with TAPS[11] and manually reviewed in GenomeStudio or Chromosome Analysis Suite (v3.3). The 13q12.2 deletion allele frequency was estimated by dividing the median log R ratio of SNPs across the deleted region with the median log R ratio of all chromosome 13 SNPs.

Whole-genome and exome data analysis

Genomic-sequencing data for cases in cohort 1 have been previously published.[3,4] For whole-genome sequencing (WGS) and WES data from TARGET (cohorts 2 and 5), methods are available at the TARGET project portal. Germline single-nucleotide variants (SNVs) were identified by the GATK4 (v4.0.11.0)[12] UnifiedGenotyper and filtered by GATK hard filters.[13] Somatic variants were called by Mutect2.[14] Structural variants were identified by Manta, Delly, and SvABA.[15-17] CNA analysis of WES data was performed using CNVkit.[18] To estimate the 13q12.2 deletion allele frequency, a sliding window approach was used (bin, 30 kb; step, 10 kb) to calculate the relative coverage ratio between tumor/matched normal samples. For Complete Genomics data, germline SNVs annotated as "VQLOW" or that were covered by <20 reads were filtered out. Somatic variants were identified by the TARGET WGS analysis pipeline. Functional annotation of variants was performed using SNPEff.[19] For cases 16 to 19 (Table 1), *FLT3* ITD was analyzed as previously described[20] and screening of all coding exons of *FLT3* was done using a targeted panel (Ampliseq System) and sequenced on an Ion S5 (Thermo Fisher Scientific). Raw data were analyzed with the Torrent browser (Thermo Fisher Scientific) and SeqNext (JSI Medical System, Los Angeles, CA). WES libraries of cases 20 to 22 (Table 1) were constructed using the Nextera DNA exome kit (Illumina) and sequenced on a NextSeq 500 (Illumina).

Fluorescence in situ hybridization

Metaphase fluorescence in situ hybridization was done on relapse samples from cases 1 and 2 (Table 1) according to standard methods using a whole-chromosome paint probe for chromosome 13 (Applied Spectral Imaging, Neckarhausen, Germany), the Vysis LSI21 probe (Abbott Laboratories, Abbott Park, IL), and the fosmid G248F80597D11.

RNA-sequencing and data analysis

RNA-sequencing (RNA-seq) data of cohort 1 (n = 152) have been published.[21] For RNA-seq data from TARGET (high-hyperdiploid, n = 37; nonhyperdiploid case with 13q12.2 deletion, n = 1), methods are available at the TARGET project portal. RNA-seq reads were mapped to human_g1k_v37 by the STAR (version 2.6.1d)[22] 2-pass mapping pipeline with WASP parameter.[23] Only reads that passed WASP filtering were used for allele-specific expression analysis. Gene expression was quantified by RNA-Seq by Expectation-Maximization (RESM)[24] and differential expression analysis was performed by the Wilcoxon rank-sum test.

Genotype phasing and allele-specific expression analysis

Genotype phasing of 13q12.2 was performed with the Sanger Imputation Service using the Haplotype Reference Consortium reference panel.[25] GATK4 ASEReadCounter was used to evaluate the allele counts of expressed heterozygous SNV sites. Heterozygous SNVs with individual allele read depths ≥10 were kept. Read counts of exonic heterozygous SNVs from the same homolog were aggregated based on the phasing results. The binomial test was applied to estimate allelic bias of exonic SNVs in the RNA-seq data against the genomic data. Allelic ratios >2 or <0.5, and values of $P < .05$ were used to identify allele-specific expression.

Chromatin structure and ChIP-seq data mining

GM12878 histone marks chromatin immunoprecipitation (ChIP)-sequencing (ChIP-seq) data (H3K27ac and H3K4me3) and DNase I–hypersensitive site sequencing (DNase-seq) data (bigwig files) were downloaded from the University of California, Santa Cruz (UCSC) database (http://genome.ucsc.edu/ENCODE/dataMatrix/encodeDataMatrixHuman.html). ETS transcription factor (ERG) and runt-related transcription factor 1 (RUNX1) ChIP-seq data were downloaded from the National Center for Biotechnology Information (NCBI) Gene Expression Omnibus (GEO) database, accession numbers GSE42075, GSE117864, and GSE138031. Proximity ligation-assisted ChIP sequencing (PLAC-seq) data, assay for transposase-accessible chromatin using sequencing (ATAC-seq) data, and ChIP-seq data (H3K27ac and H3K4me3) from the ALL cell line NALM-6 were obtained from GEO, accession number GSE126300.[26] Raw reads were aligned to human_g1k_v37 using the Burrows-Wheeler Aligner (BWA)[27] and signal tracks were generated using deeptools.[28]

DS1, DS2, and DS3 motif scanning

Motif scanning of the DNaseI hypersensitive site (DS)1, DS2, and DS3 regulatory elements was done with the GimmeMotifs (v0.12.0).[29] Initally, "gimme scan" was run with hg19 as reference, against the GimmeMotifs default motif database gimme.vertebrate.v5.0, derived from the Catalog of Inferred Sequence Binding Preferences (CIS-BP) database.[30] To specifically scan for ERG and RUNX motifs, a custom position weight matrix file, containing 3 ERG motifs and 8 RUNX motifs (supplemental Table 1 and supplemental Figure 2), was generated from ERG and RUNX position weight matrices from the gimme.vertebrate.v5.0, HOMER,[31] and Jaspar CORE[32] databases.

Hi-C data analysis

Previously published high-resolution chromosome conformation capture (Hi-C) data from 6 primary BCP ALL samples, including 1

Table 1. 13q12.2 deletions in 27 cases of ALL

Case	Deleted region*	Size, bp	*FLT3* mutation	Deletion at diagnosis	Deletion at relapse
1	chr13:28 689 519-28 818 033†	128 514	p.A680V	Yes	Yes
2	chr13:28 686 699-28 818 553†	131 854	No	Yes	Yes
3	chr13:28 691 097-28 795 606	104 509	p.D835Y	Yes	N/A
4	chr13:28 675 905-28 816 917†	141 012	p.I867S	Yes	N/A
5	chr13:28 678 803-28 814 370	135 567	No	Yes	N/A
6	chr13:28 689 487-28 818 033†	128 546	No	Yes	N/A
7	chr13:28 675844-28 779 095†	103 251	ITD	Yes	N/A
8	chr13:28 678 544-28 717 233†	38 689	No	Yes	N/A
9	chr13:28 672 989-28 816 869†	143 880	No	Yes	N/A
10	chr13:28 681 356-28 816 438	135 082	NK	Yes	N/A
11	chr13:28 681 356-28 816 438	135 082	NK	Yes	N/A
12	chr13:28 675 878-28 817 064†	141 186	No	Yes	N/A
13	chr13:28 682 922-28 798 410†	115 488	No	Yes	No
14	chr13:28 706 767-28 749 112†	42 345	No	No	Yes
15	chr13:28 675 750-28 835 054†	159 304	p.M837P	Yes	Yes
16	chr13:28 685 061-28 813 774	128 713	No	Yes	N/A
17	chr13:28 689 100-28 801 000	111 900	p.R834dup	Yes	N/A
18	chr13:28 689 223-28 722 472	33 249	No	Yes	N/A
19	chr13:28 690 533-28 829 444	138 911	No	Yes	N/A
20	chr13:28 691 097-28 828 603	137 506	No	Yes	N/A
21	chr13:28 719 402-28 814 420	95 018	No	Yes	N/A
22	chr13:28 687 654-28 759 548	71 894	ITD	Yes	N/A
23	chr13:28 712 891-28 813 915	101 024	No	Yes	N/A
24	chr13:28 712 891-28 813 915	101 024	No	Yes	N/A
25	chr13:28 712 685-28 830 678	117 993	No	Yes	N/A
26	chr13:28 712 435-28 752 128	39 693	p.S838_D839insEG/p.N841T	Yes	N/A
27	chr13:28 712 685-28 813 851	101 166	p.L576P	Yes	N/A

bp, base pair; N/A, data not available (no relapse or no sample available); NK, not known.

*Minimally deleted region based on SNP array analysis or WES copy number data unless otherwise indicated.

†Breakpoint validated by WGS.

sample with 13q12.2 deletion (#3 in the present study; Table 1), were used to investigate the chromatin interaction at the 13q12.2 locus.[3] To achieve high-resolution chromatin-interactions maps, the previously constructed Hi-C libraries from 2 of the high-hyperdiploid cases,[3] including #3, were resequenced on a NovaSeq (Illumina), with 1.5 billion pair-end reads obtained for each sample. Paired-end reads were mapped to human_g1k_v37 using Juicer.[33] Hi-C data of the GM12878 and NALM-6 cell lines were downloaded from GEO (accession numbers GSE63525 and GSE115491, respectively). All .hic files were converted into 25-kb read count matrices. Reads mapped to the same or adjacent bins were removed. The filtered contact matrices were normalized by the chromosome-adjusted iterative correction procedure.[34] Standardized genome-wide chromosome-adjusted iterative correction procedure scores (Z scores) were used for interaction frequency analysis. Additionally, multiHiCcompare was used to detect differential chromatin interactions.[35] Insulation score[36] calculations were performed as described in Yang et al.[3]

Results

Hemizygous 13q12.2 microdeletions are recurrent in BCP ALL

Overall, hemizygous 13q12.2 deletions were identified in 27 of 1418 BCP ALL cases in the 5 cohorts (Table 1). The deletion size varied from 39 kb to 160 kb, with a median size of 129 kb (Figure 1A). The majority of the proximal breakpoints were located immediately upstream of the *FLT3* gene, whereas the distal breakpoints mapped to introns 6 (20 of 27; 74%), 5 (3 of 27; 11%), 1 (2 of 27; 7.4%), 2 (1 of 27; 3.7%), and 8 (1 of 27; 3.7%) of the *PAN3* gene. Metaphase fluorescence in situ hybridization in 2 cases and WGS in 11 cases confirmed that the CNAs in the region were due solely to interstitial deletions and not associated with other structural rearrangements (Table 1; supplemental Figure 3). The deletions could be confirmed to be somatic in 23 of 27 cases based on comparison with a matched normal sample (#1-2, #4-15, and #20-27) or because of a small residual signal from the normal cells in the SNP array analysis (#3). Two cases (#6 and #7) harbored subclonal deletions (estimated to <10% of the cells). One case (#16) had trisomy 13 as well as 2 different 13q12.2 deletions, thus retaining 1 copy of this segment (supplemental Figure 4). Of the 27 cases with 13q12.2 deletions, paired diagnostic and relapse samples were available from 5 cases. Three of these had the same deletion at both diagnosis and relapse, 1 case lost the deletion at relapse, and 1 case harbored the deletion at relapse but not at diagnosis (Table 1). Among 25 investigated cases with 13q12.2 deletions, *FLT3* mutations were identified in 9 (36%) (Table 1).

13q12.2 deletions are enriched in the high-hyperdiploid ALL subgroup and associated with relapse

We next investigated the cytogenetic and clinical features of cases with 13q12.2 deletions. Among 9 cases with 13q12.2 deletions in cohort 1, 7 were high hyperdiploid (7 of 110; 6.4%) and 2 (2 of 166; 1.2%) were non–high-hyperdiploid ($P = .046$; 2-tailed Fisher exact test). Similarly, in cohort 2, deletions were identified in 4 of 120 high-hyperdiploid (2.7%) and 2 of 663 non–high-hyperdiploid (0.3%) cases ($P = .012$; 2-tailed Fisher exact test). The 4 cases with deletions that were not high hyperdiploid in cohorts 1 and 2 comprised 1 *ETV6/RUNX1*$^+$ case, 2 cases with intrachromosomal amplification of chromosome 21 (iAMP21), and 1 B-other case (Table 2). Further investigations of 3 validation cohorts showed that 13q12.2 deletions were identified in 4 of 123 (3.3%; cohort 3), 3 of 97 (3.1%; cohort 4), and 5 of 139 (3.6%; cohort 5) high-hyperdiploid cases, respectively. Overall, the frequency of 13q12.2 deletions was 3.9% in high-hyperdiploid cases and 0.48% in non-hyperdiploid pediatric BCP ALL ($P = 6.4 \times 10^{-6}$, 2-tailed Fisher exact test). Thus, although 13q12.2 deletions were not restricted to high-hyperdiploid ALL, they were clearly more common in this subtype compared with other BCP ALL subtypes.

Of the 27 cases with 13q12.2 deletions, 18 were female, giving a male-to-female ratio of 0.50 (Table 2). Restricting the analysis to the 23 high-hyperdiploid cases increased this ratio to 0.64 (14 female). The median age at diagnosis was 6 years for all patients (range, 2-17 years) and 5 years for high-hyperdiploid patients (range, 2-17 years) (Table 2). The median white blood cell count was 6.3×10^9/L for all cases and the same for high-hyperdiploid cases only (range, 1.1-118 and 1.2-118, respectively).

We have previously reported that 13q12.2 deletions were enriched at diagnosis in cases that subsequently suffered leukemia relapse in cohort 1.[5] To see whether this held true in an independent cohort, we analyzed data from cohort 2. 13q12.2 deletions were seen in 3 of 90 cases (3.3%) that relapsed and 3 of 690 cases (0.43%) that did not ($P = .045$; 2-tailed Fisher exact test), in line with the data from cohort 1.

13q12.2 deletions lead to upregulation of *FLT3* in *cis*

The only gene in the 13q12.2-deleted region is *PAN3*, a regulatory subunit of the PAN2-PAN3 complex, involved in messenger RNA decay.[37] The deletions comprised 1 (n = 2) or more exons (n = 25) of *PAN3*, including its promoter (Figure 1). To investigate whether the 13q12.2 deletions affect the expression of the *PAN3* gene, differential expression analyses was performed on RNA-seq data. To avoid potential gene-expression bias between different subtypes of BCP ALL and gene-dosage effects caused by CNAs, we restricted this analysis to high-hyperdiploid ALL cases with disomy 13 (n = 83). Hemizygous deletions of 13q12.2 led to a somewhat reduced expression of *PAN3* but this effect was not statistically significant ($\log_2$ fold change = −0.285; $P = .27$), indicating that *PAN3* expression is rescued by expression of the retained allele (Figure 2). Because *FLT3* is located immediately proximally to the 13q12.2 deletions, we next examined whether the expression of this gene was affected. Significantly higher expression of *FLT3* ($\log_2$ fold change = 0.55; $P = .025$) was detected in cases with 13q12.2 deletions (n = 8) compared with cases lacking the deletion (n = 75), indicating that the deletions lead to increased expression of *FLT3* in high-hyperdiploid ALL (Figure 2). This difference remained when cases with *FLT3* mutations were excluded ($P = .028$; supplemental Figure 5A). There was no difference in *FLT3* expression between cases with and without *FLT3* mutation in cases lacking 13q12.2 deletion (supplemental Figure 5) or between female and male patients (supplemental Figure 6).

We next performed allele-specific expression analysis of *FLT3*. Of 77 informative BCP ALL cases with expression of exonic heterozygous SNVs detectable by RNA-seq, 9 harbored 13q12.2 deletions. Significant allele expression bias for *FLT3* was seen in the 7 cases with clonal 13q12.2 deletions, whereas the 2 cases with subclonal deletions as well as cases lacking the deletion did not show allele-expression bias (Figure 3A).

To ascertain whether it was the *FLT3* allele on the chromosomal homolog harboring the deletion that was preferentially expressed (consistent with a *cis* effect) or the other *FLT3* allele (a *trans* effect), SNP array data and WGS data were phased to build a haplotype scaffold of the 13q12.2 locus for each case. Six cases were informative in this analysis (ie, carried at least 2 heterozygous SNVs in the deleted region and at least 1 expressed heterozygous SNV in *FLT3* exons). Per the analysis, all cases showed an upregulation of the *FLT3* allele that was on the chromosome 13 homolog with the deletion, that is, a *cis* effect (supplemental Table 2).

To investigate the association between *FLT3* mutations and 13q12.2 deletions, we analyzed the expression of the mutated alleles. Among the 9 informative BCP ALL cases with expression of somatic *FLT3* mutations detectable by RNA-seq, significantly

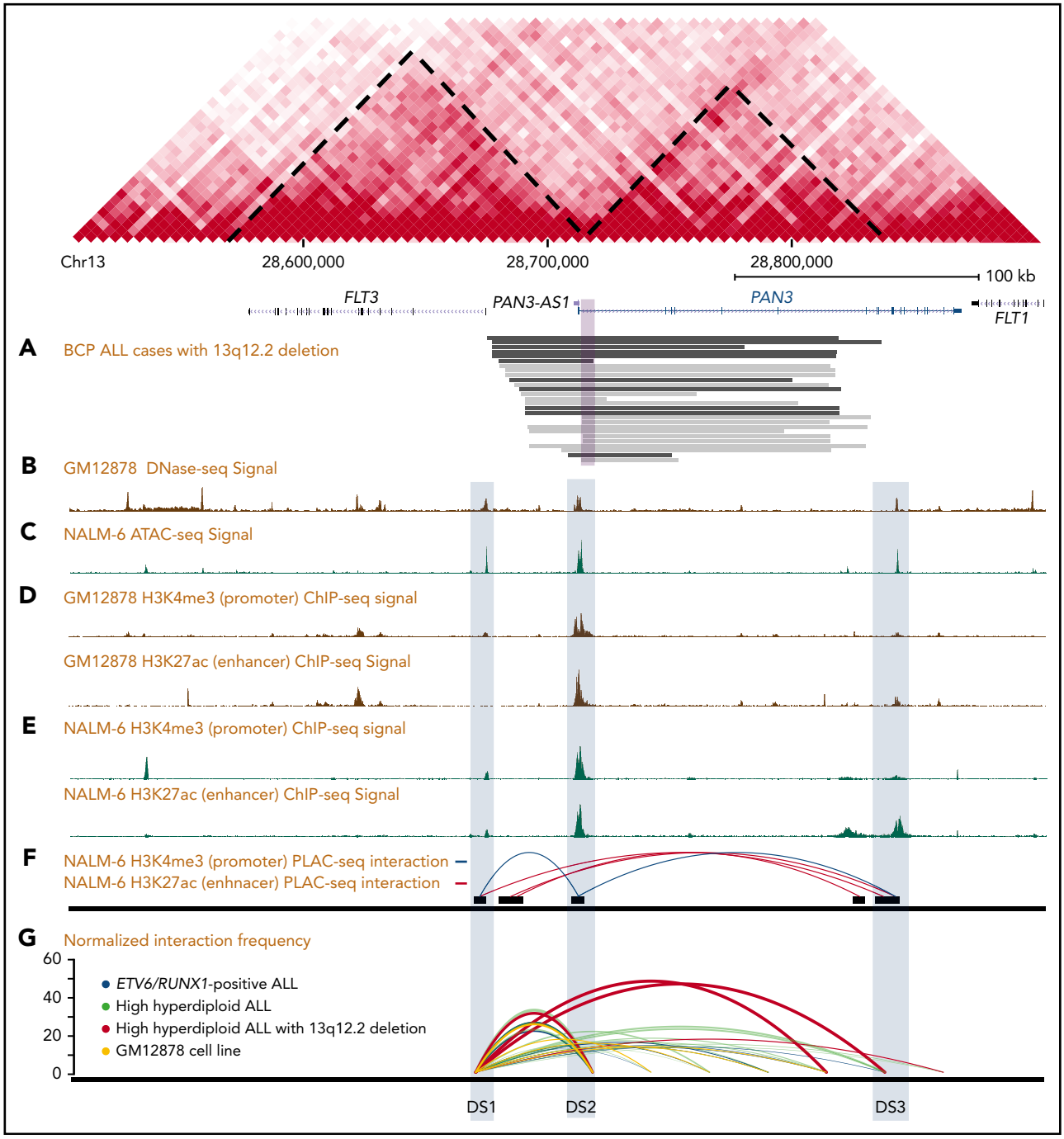

Figure 1. Genetic mapping and epigenetic landscape of the 13q12.2 locus. Map of the *FLT3* and *PAN3* loci in 13q12.2. Predicted topologically associating domains based on data from the lymphoblastic GM12878 cell line are indicated by diagonal dashed lines. (A) Hemizygous deletions identified in 27 BCP ALL samples by WGS (black) or SNP array or WES (gray). The violet square corresponds to the minimally deleted region. (B) DNase-seq signal based on the GM12878 cell line. (C) ATAC-seq signal based on the NALM-6 cell line. (D) ChIP-seq of histone modifications (H3K27ac and H3K4me3) based on the GM12878 (E) and the NALM-6 cell lines. (F) H3K27ac- and H3K4me3-enriched PLAC-seq interaction map based on the NALM-6 cell line. (G) Relative interaction frequencies in 13q12.2 in 6 primary ALL cases and the GM12878 cell line based on Hi-C, where higher values on the y-axis correspond to stronger interaction. Increased interactions with the enhancer element DS3 are seen in the case with 13q12.2 deletion.

higher expression of the *FLT3* mutation was detected in cases that carried 13q12.2 deletions (n = 3), in contrast to cases lacking 13q12.2 deletions (n = 6) (Figure 3B). This indicates that the *FLT3* mutations were in the same chromosomal homolog as the 13q12.2 deletions and that the deletions lead to increased expression of the mutated alleles. Analyzing the predicted clonality of *FLT3* mutations and 13q12.2 deletions in cases that harbored both revealed that the mutation and deletion were present at similar frequencies in the majority of cases, and thus likely present in the same clone (supplemental Figure 7). In 1 case each, the mutation and the deletion were found in a larger proportion of the cells. Furthermore, in 1 case, the mutation was missing in the relapse sample, showing that the deletion arose first.

Table 2. Clinical and cytogenetic data of 27 cases of ALL with 13q12.2 deletions

Case*	Cohort	Sex	Age, y	WBC count, $\times 10^9$/L	Genetic subtype	Karyotype at diagnosis
1†	1	M	3	51	HeH	55,XY,+X,+4,+5,+6,idic(7)(p11),+8,+10,+14,+17,+21
2†	1	F	5	6.3	HeH	53,XX,+4,+6,+10,+14,+18,+21,+21
3†	1	F	3	19	HeH	55,XX,+X,+4,+6,+7,+10,+14,+17,+18,+21
4†	1	M	5	2.0	HeH	59,XXY,−1,−2,−3,−7,−9,−11,−12,−13,+14,−16,−19,−20,+21
5†	1	F	6	1.2	HeH	53,XX,+X,+4,+6,+8,+10,+14,+17,+21,+21
6†	1	F	15	3.5	HeH	57,XX,+X,+X,+4,+6,der(8)t(8;14)(p11; q12),+10,+14,+14,+17,+18,+21,+21
7†	1	M	4	17	HeH	57,XY,+X,+3,+4,+6,+8,+10,+14,+16,+18,+21/55-57,idem,i(7)(q10)
8†	1	F	11	6.1	iAMP21	45-47,XX,del(5)(p13),−7,−8,−19,qdp(21)(q22q22),+r,+1-2mar,inc
9†	1	F	4	12	*ETV6/RUNX1*	46,XX,del(12)(p13p13),t(12;21)(p13;q22)
10	2	F	17	19	B-other	N/A
11	2	F	10	5.6	HeH	N/A
12	2	M	17	2.1	HeH	57,XY,+X,+4,+6,+9,+10,+14,+14,+18,+21,+21,+mar
13	2	F	7	3.6	HeH	N/A
14	2	F	2	1.3	HeH	53,XX,+X,+6,+14,+15,+17,+21,+21
15	2	F	12	1.1	iAMP21	N/A
16	3	M	4	18	HeH	53,XY,+X,+4,+6,+13,+18,+21,+21‡
17	3	F	5	6.3	HeH	53,XX,+X,+4,+4,+6,+14,+21,+21/54,idem,+17‡
18	3	M	3	27	HeH	52,XY,+X,+6,+14,+17,+18,+21,+21‡
19	3	F	4	9.9	HeH	54,XX,+X,+X,+6,+10,+14,+18,+21,+21‡
20	4	M	4	2.0	HeH	52,XY,+X,+4,+6,+14,+21,+21‡
21	4	F	4	4.8	HeH	54,XX,+X,+4,+6,+14,+17,+18,+21,+21‡
22	4	M	10	1.4	HeH	54,XY,+X,+4,+10,+14,+14,+20,+21,+21/56,idem,+8,+9‡
23	5	M	12	36	HeH	57,XY,+X,+1,add(1)(p13),del(1)(q42),+3,+4,+6,+7,del(7)(q22),+10, −12,+14,+14,i(17)(q10),+21,+21,+mar
24	5	F	7	7.2	HeH	54,XX,+X,dup(1)(q21q32),+4,+6,+10,+14,+17,+18,+21
25	5	F	13	18	HeH	55,XX,+X,+X,dup(1)(q25q44),+4,+6,+10,+14,+17,+18,+21
26	5	F	6	29	HeH	53,XX,+X,+4,+6,+9,+14,+21,+21/53,idem,−9,+der(9;17)(q10;q10)
27	5	F	13	118	HeH	56,XX,+X,+4,+6,+8,+10,+11,+14,+14,+21,+21

F, female; HeH, high-hyperdiploid; iAMP21, intrachromosomal amplification of chromosome 21; M, male; N/A, data not available; WBC, white blood cell.

*Cases 10-15 correspond to TARGET cases PANPRP, PANVUV, PAPHCJ, PARBRK, PAPJIB, and PARSZH, respectively. Cases 23-27 correspond to TARGET cases PARDXI, PARFJK, PARRVI, PAPAMH, and PARKZX, respectively.

†The karyotypes of cases 1-9 have been previously published in Olsson et al.[7]

‡Based on SNP array data only.

Functional annotation of 13q12.2 regulatory elements

Considering our finding that 13q12.2 deletions are associated with upregulation of *FLT3* expression in *cis*, we next examined the regulatory elements at this locus. Using publicly available DNase-seq and ATAC-seq data, 3 open chromatin regions were identified in the region: DS1 (*FLT3* promoter, chr13:28 674 500 to 28 675 000), DS2 (chr13:28 710 000 to 28 715 000), and DS3 (*PAN3* intron 8; chr13:28 843 000 to 28 843 500) (Figure 1B-C). The 13q12.2 deletions resulted in loss of DS2. Further examination

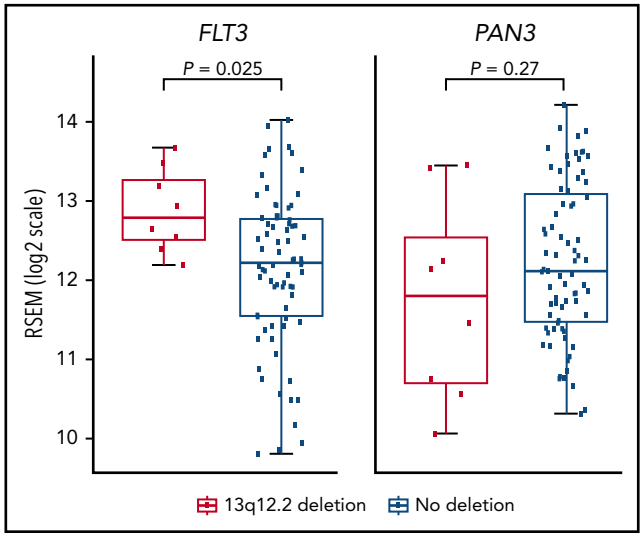

Figure 2. Gene-expression analysis of high-hyperdiploid cases with 13q12.2 deletions. RNA expression of the *FLT3* and *PAN3* genes in cases with and without 13q12.2 deletions.

of publicly available ChIP-seq data of the histone modifications H3K4me3 (marks of promoters) and H3K27ac (marks of active enhancers) showed that the H3K4me3 signal was enriched at DS1 and DS2 and the H3K27ac signal at DS2 and DS3 (Figure 1D-E), respectively. Further analysis of H3K4me3-enriched PLAC-seq data showed interactions between DS1 and DS2, whereas long-range interactions between DS1 and DS3 were observed in H3K27ac-enriched data (Figure 1F).[26] These data indicate that DS2 and DS3 both act as enhancers for *FLT3*. Transcription factor–binding sites in these regions are given in supplemental Table 3. A targeted search for sequences commonly bound by RUNX1 and ERG showed a number of moderately strong hits (supplemental Table 4) and ChIP-seq data showed that the RUNX1 signal was enriched in all 3 regions whereas the ERG signal was enriched in DS1 and DS2 (supplemental Figure 8).

Hi-C data from ALL cell lines showed that the 13q12.2 locus is divided into 2 topologically associating domains (TADs), 1 harboring *FLT3* and the other *PAN3*, with a TAD border at approximately chr13:28 710 000 to 28 715 000 (Figure 4A). The 13q12.2 deletions overlap with this TAD boundary (Figure 1). Analysis of high-resolution contact matrices from 2 primary high-hyperdiploid ALL, 1 without 13q12.2 deletion and 1 with, revealed that the case without deletion displayed similar TADs as in the cell lines whereas the ALL with deletion had lost these TADs (Figure 4A). To address this further, we analyzed the insulation score profile of previously published primary BCP ALL Hi-C data, in total 6 cases, including the case with 13q12.2 deletion.[3] This showed that the deletion resulted in significant changes in the local insulation score profile, indicating that the 3-dimensional genome organization was disrupted in this region (Figure 4B). Increased interaction frequencies between DS1 and DS3 were also seen in the case with 13q12.2 deletion compared with samples lacking the deletion (Figure 1G). This finding was confirmed by statistical analysis of contact matrices from all samples, showing that the 13q12.2 deletion in case 3 significantly increased the interaction frequencies between DS1 and DS3 (false discovery rate <.01; supplemental Table 5). No differences were detected in contact matrices in chromosome 13 between female and male patients in BCP ALL samples without 13q12.2 deletion (supplemental Table 6). Taken together, our data demonstrate a novel *cis*-acting mechanism in which deletion of a TAD border and regulatory element DS2 leads to increased expression of the *FLT3* allele located directly at the proximal end of the deletion via increased interactions with the DS3 enhancer (Figure 4C).

Discussion

In this study, we performed a comprehensive genomic, transcriptomic, and chromatin architecture analysis of BCP ALL cases to investigate the frequency of 13q12.2 deletions and their pathological impact. Despite the loss of 1 copy of the *PAN3*

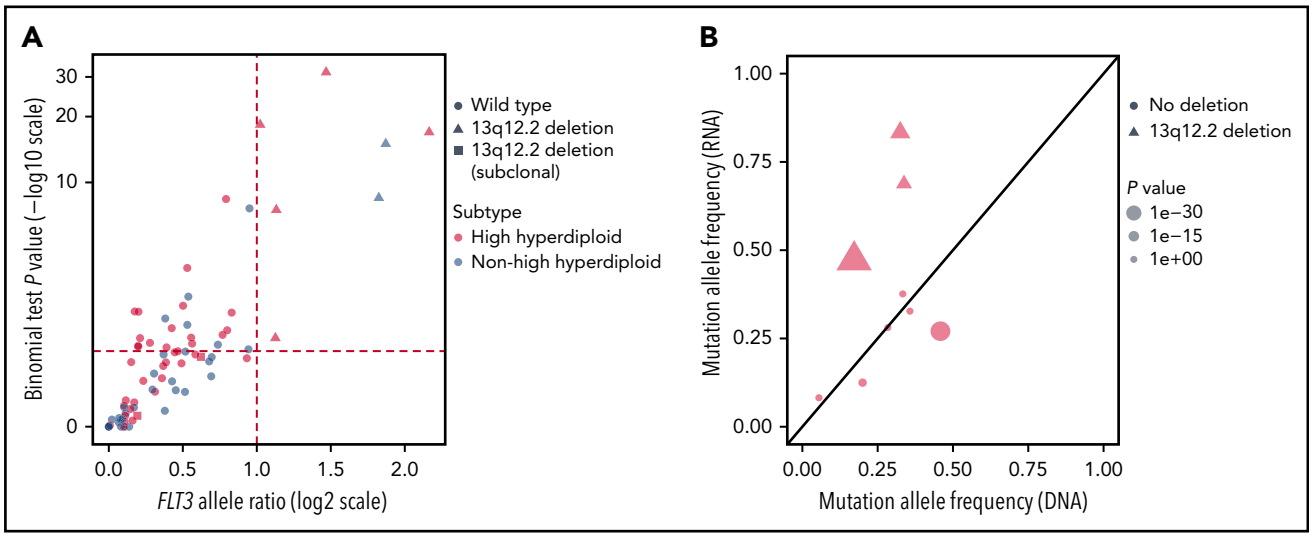

Figure 3. Allele-specific expression analysis of *FLT3* in BCP ALL. (A) Scatterplot of allelic ratio (x-axis) and log-scale binomial *P* values (y-axis) of *FLT3* in BCP ALL (n = 77) with informative SNVs. The horizontal line represents the binomial *P* value of .05 ($\log_{10}$ scale) and the vertical lines represent the ratio for the expressed reference/nonreference allele ($\log_2$ scale). All 7 cases with clonal 13q12.2 deletions displayed allele-specific expression of *FLT3* (top right quadrant). (B) *FLT3* mutant allele frequencies observed by RNA-seq (y-axis) and by genomic-sequencing data (x-axis) of 9 BCP ALL cases. The line y=x is shown in black. The 3 cases with concurrent *FLT3* mutation and 13q12.2 deletion showed increased expression of the mutated allele.

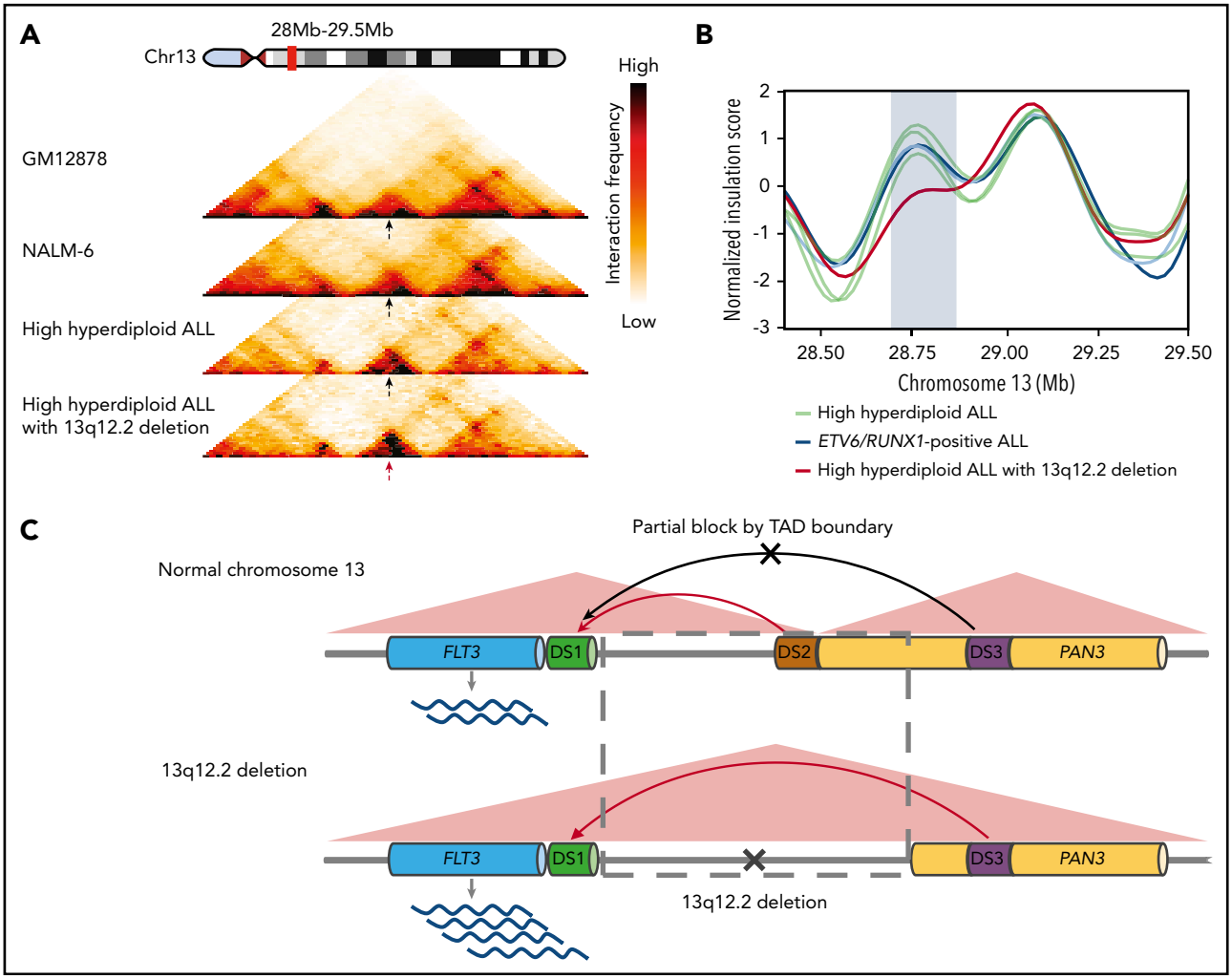

Figure 4. Changes in TADs and enhancer hijacking in ALL with 13q12.2 deletion. (A) Juicer KR-normalized Hi-C interaction heatmaps at 13q12.2 (chr13:28.0 to 29.5 Mb) of the GM12878 cell line, the NALM-6 cell line, and 2 primary high-hyperdiploid ALL cases (25-kb resolution). The black arrows indicate the TAD boundary between DS1 and DS3 and the red arrow indicates the disruption of this TAD boundary in the case with 13q12.2 deletion (case 3). (B) Insulation score profile at 13q12.2 derived from chromatin interaction sequencing of 6 primary ALL cases. The case with 13q12.2 deletion (case 3) displays a deviant insulation score in this region (blue rectangle), corresponding to aberrant chromatin organization likely due to loss of a TAD boundary. (C) Schematic figure of chromatin remodeling and enhancer hijacking in ALL with 13q12.2 deletion. In normal hematopoietic cells, *FLT3* expression is primarily controlled by interactions between the *FLT3* promoter element DS1 with the DS2 enhancer located in the 5′ region of *PAN3* (top panel). In cells with 13q12.2 deletion, a TAD boundary is lost together with DS2, resulting in increased interactions between DS1 and the upstream enhancer element DS3, thereby upregulating *FLT3* messenger RNA expression (bottom panel).

gene, we found no clear effect on its expression. Instead, we found that the breakpoints of the 13q12.2 deletions occur immediately 5′ to the *FLT3* promoter. Considering that *FLT3* mutations are well-known driver events in leukemia, we focused our studies on investigating the possible role of 13q12.2 deletions in dysregulation of *FLT3* gene expression. We here show that the deletions disrupt the TAD structure and change promoter-enhancer interactions in the region, leading to increased expression of the *FLT3* allele encoded on the same chromosomal homolog (Figure 4C). Such enhancer hijacking has recently been reported for the *IRS4* gene in lung cancer, sarcoma and squamous cell cancer, the *CCNE1* and *IGF2* genes in gastric cancer, and the *TAL1* and *LMO2* genes in T-ALL,[38-40] but it is not yet known how common this mechanism is in tumorigenesis. Our data demonstrate, for the first time, that 13q12.2 deletions lead to *FLT3* overexpression via chromatin remodeling and enhancer hijacking in leukemia and reveal new details of normal *FLT3* regulation in hematopoietic cells.

High levels of *FLT3* expression have been shown to be associated with FLT3 phosphorylation in leukemia, resulting in putative ligand-independent activation of the receptor.[41,42] Thus, the 13q12.2 deletions are expected to result in activated downstream FLT3 signaling. Furthermore, high *FLT3* expression has been reported to be a poor prognostic sign in both ALL and AML.[42-45] In line with this, we found a higher frequency of relapses in cases with 13q12.2 deletions in 2 independent cohorts treated on different protocols. However, larger prospective studies are needed to determine whether 13q12.2 deletions could be used as a prognostic indicator in ALL.

We have previously reported that 13q12.2 deletions are associated with high-hyperdiploid ALL.[5] Here, we could validate this in an independent data set. This strongly suggests that recurrent 13q12.2 deletions play a particular pathogenetic role in high-hyperdiploid ALL development. Notably, even though *FLT3*

levels are generally high in this subgroup, cases with deletions still had significantly increased expression. Together with the fact that *FLT3* mutations are particularly common in high-hyperdiploid cases,[4,46] this further indicates that *FLT3* is a strong driver in the leukemogenesis of high-hyperdiploid ALL.

The basis for 13q12.2 deletions being enriched in high-hyperdiploid ALL is not known. Interestingly, 2 of the 4 non-hyperdiploid cases with 13q12.2 deletion belonged to the iAMP21 ALL subtype. iAMP21 is generally seen in only 2% of pediatric BCP ALL,[47] indicating that 13q12.2 deletions could also be enriched in this subgroup. Both high-hyperdiploid and iAMP21 ALL have gain of parts of chromosome 21, including the region containing the genes encoding the RUNX1 and ERG hematopoietic transcription factors. Interestingly, we detected putative binding sites for RUNX1 in the DS2 and DS3 regulatory regions, and ALL cell line ChIP-seq data showed RUNX1 binding to these regions. It is thus possible that RUNX1 plays a role in the strong association between 13q12.2 deletions and high-hyperdiploid/iAMP21 leukemia but further functional studies are needed to substantiate this.

There were more female than male patients with 13q12.2 deletion both overall and in high-hyperdiploid cases only. BCP ALL is somewhat more common in male patients,[48] whereas the high-hyperdiploid subtype is equally common in female and male patients.[49] We could not detect a difference in chromatin interactions in chromosome 13 or *FLT3* expression levels between female and male patients, indicating that gene regulation in the 13q12.2 locus is similar between the sexes. Taken together, further studies of larger cohorts of ALL with 13q12.2 deletion are needed to determine whether the skewed sex ratio detected in this study was incidental or corresponds to a true biological phenomenon.

Previous studies have shown that *FLT3* ITD and activating mutations are associated with upregulation of *FLT3* expression in AML.[41,42] Moreover, in AML, *FLT3* mutations are rendered homozygous via somatic uniparental isodisomy of 13q in a proportion of the cases, indicating that increased expression levels of *FLT3* mutations contribute to leukemia development.[42,43] We could not detect higher *FLT3* expression in cases with *FLT3* mutations lacking 13q12.2 deletion. However, 3 ALL cases with concurrent 13q12.2 deletions and *FLT3* mutations showed significantly higher expression of the *FLT3*-mutated alleles, suggesting a potential selective advantage of the *FLT3* mutant clone with 13q12.2 deletions through increased expression of the mutation. Analysis of the clonal composition of leukemia with concurrent *FLT3* mutations and 13q12.2 deletions showed that either the mutation or the deletion could occur first, indicating that these aberrations do not occur in a specific order.

The precise timing of the 13q12.2 deletions in BCP ALL vary among cases. Of 5 paired diagnostic-relapse samples with 13q12.2 deletions, 3 shared the deletion, suggesting that it was present in the leukemic founder clone. On the other hand, 1 case with paired diagnostic-relapse samples harbored the deletion only in the diagnostic clone, whereas another had it only in the relapse clone, suggesting a later occurrence. Furthermore, 1 case with trisomy 13 harbored different deletions in 2 of the chromosomal homologs, showing that at least 1 of the deletions must have occurred after the gain of this chromosome. Finally, 2 cases had subclonal deletions, indicating that the deletion occurred at later stages of the leukemic evolution. Thus, the 13q12.2 deletion appears to give a selective advantage to the leukemic cell regardless of the stage at which it arises.

In summary, our study describes a novel way of *FLT3* involvement in leukemogenesis by upregulation via enhancer hijacking. These data further highlight the role of *FLT3* as a driver event in the development of high-hyperdiploid BCP ALL.

Acknowledgments

The results published here are in part based upon data generated by the Therapeutically Applicable Research to Generate Effective Treatments (TARGET) Initiative (phs000464). The TARGET data used for this analysis are available at https://portal.gdc.cancer.gov/projects. Information about TARGET can be found at https://ocg.cancer.gov/programs/target.

This work was supported by grants from the Swedish Cancer Society (CAN 2017/291 [B.J.]; CAN 2016/497 [K.P.]), the Swedish Childhood Cancer Foundation (TJ2018-0061 [M.Y.]; PR2018-0004 [B.J.]; PR2018-0023 [K.P.]), the Swedish Research Council (2016-01084 [B.J.]; 2016-01459 [K.P.]), the Ministry of Health of the Czech Republic (Czech Health Research Council; #15-30626A [M.Z.]), the University Hospital Motol (#00064203 [M.Z., J.Z.]), governmental funding of clinical research within the National Health Service (ALFSKANE-623431 [K.P.]), and the Royal Physiographic Society of Lund (M.Y.).

Authorship

Contribution: M.Y., L.O.-A., J.U., and K.H.N. analyzed data; S.S. and E.L.W. performed experiments; N.D., M.S., M.Z., J.Z., T.F., and B.J. provided resources and analyzed data; K.P. supervised the study; and M.Y. and K.P. designed the study and wrote the article with input from all authors.

Conflict-of-interest disclosure: The authors declare no competing financial interests.

ORCID profiles: M.Y., 0000-0002-3324-1498; N.D., 0000-0002-3927-1022; J.U., 0000-0002-2190-3896; K.H.N., 0000-0002-2397-2254; K.P., 0000-0001-7950-222X.

Correspondence: Kajsa Paulsson, Division of Clinical Genetics, Lund University, BMC C13, SE-221 84 Lund, Sweden; e-mail: kajsa.paulsson@med.lu.se.

Footnotes

Submitted 23 December 2019; accepted 20 April 2020; prepublished online on *Blood* First Edition 8 May 2020. DOI 10.1182/blood.2019004684.

Publicly available data sets used in this study are available as specified in the different subsections. The remaining data sets are available from the corresponding author upon reasonable request.

The online version of this article contains a data supplement.

There is a *Blood* Commentary on this article in this issue.

The publication costs of this article were defrayed in part by page charge payment. Therefore, and solely to indicate this fact, this article is hereby marked "advertisement" in accordance with 18 USC section 1734.

REFERENCES

1. Annesley CE, Brown P. The biology and targeting of FLT3 in pediatric leukemia. *Front Oncol*. 2014;4:263.
2. Armstrong SA, Mabon ME, Silverman LB, et al. FLT3 mutations in childhood acute lymphoblastic leukemia. *Blood*. 2004;103(9):3544-3546.
3. Yang M, Vesterlund M, Siavelis I, et al. Proteogenomics and Hi-C reveal transcriptional dysregulation in high hyperdiploid childhood acute lymphoblastic leukemia. *Nat Commun*. 2019;10(1):1519.
4. Paulsson K, Lilljebjörn H, Biloglav A, et al. The genomic landscape of high hyperdiploid childhood acute lymphoblastic leukemia. *Nat Genet*. 2015;47(6):672-676.
5. Olsson L, Castor A, Behrendtz M, et al. Deletions of IKZF1 and SPRED1 are associated with poor prognosis in a population-based series of pediatric B-cell precursor acute lymphoblastic leukemia diagnosed between 1992 and 2011. *Leukemia*. 2014;28(2):302-310.
6. Panagopoulos I, Gorunova L, Andersen HK, et al. PAN3-PSMA2 fusion resulting from a novel t(7;13)(p14;q12) chromosome translocation in a myelodysplastic syndrome that evolved into acute myeloid leukemia. *Exp Hematol Oncol*. 2018;7:7.
7. Olsson L, Lundin-Ström KB, Castor A, et al. Improved cytogenetic characterization and risk stratification of pediatric acute lymphoblastic leukemia using single nucleotide polymorphism array analysis: A single center experience of 296 cases. *Genes Chromosomes Cancer*. 2018;57(11):604-607.
8. Duployez N, Abou Chahla W, Lejeune S, et al. Detection of a new heterozygous germline ETV6 mutation in a case with hyperdiploid acute lymphoblastic leukemia. *Eur J Haematol*. 2018;100(1):104-107.
9. Zaliova M, Hovorkova L, Vaskova M, Hrusak O, Stary J, Zuna J. Slower early response to treatment and distinct expression profile of childhood high hyperdiploid acute lymphoblastic leukaemia with DNA index <1.16. *Genes Chromosomes Cancer*. 2016;55(9):727-737.
10. Wang K, Li M, Hadley D, et al. PennCNV: an integrated hidden Markov model designed for high-resolution copy number variation detection in whole-genome SNP genotyping data. *Genome Res*. 2007;17(11):1665-1674.
11. Rasmussen M, Sundström M, Göransson Kultima H, et al. Allele-specific copy number analysis of tumor samples with aneuploidy and tumor heterogeneity. *Genome Biol*. 2011;12(10):R108.
12. DePristo MA, Banks E, Poplin R, et al. A framework for variation discovery and genotyping using next-generation DNA sequencing data. *Nat Genet*. 2011;43(5):491-498.
13. Thomas GWC, Wang RJ, Puri A, et al. Reproductive longevity predicts mutation rates in primates. *Curr Biol*. 2018;28(19):3193-3197.e5.
14. Cibulskis K, Lawrence MS, Carter SL, et al. Sensitive detection of somatic point mutations in impure and heterogeneous cancer samples. *Nat Biotechnol*. 2013;31(3):213-219.
15. Chen X, Schulz-Trieglaff O, Shaw R, et al. Manta: rapid detection of structural variants and indels for germline and cancer sequencing applications. *Bioinformatics*. 2016;32(8):1220-1222.
16. Rausch T, Zichner T, Schlattl A, Stütz AM, Benes V, Korbel JO. DELLY: structural variant discovery by integrated paired-end and split-read analysis. *Bioinformatics*. 2012;28(18):i333-i339.
17. Wala JA, Bandopadhayay P, Greenwald NF, et al. SvABA: genome-wide detection of structural variants and indels by local assembly. *Genome Res*. 2018;28(4):581-591.
18. Talevich E, Shain AH, Botton T, Bastian BC. CNVkit: genome-wide copy number detection and visualization from targeted DNA sequencing. *PLOS Comput Biol*. 2016;12(4):e1004873.
19. Cingolani P, Platts A, Wang L, et al. A program for annotating and predicting the effects of single nucleotide polymorphisms, SnpEff: SNPs in the genome of Drosophila melanogaster strain w1118; iso-2; iso-3. *Fly (Austin)*. 2012;6(2):80-92.
20. Kiyoi H, Naoe T, Nakano Y, et al. Prognostic implication of FLT3 and N-RAS gene mutations in acute myeloid leukemia. *Blood*. 1999;93(9):3074-3080.
21. Lilljebjörn H, Henningsson R, Hyrenius-Wittsten A, et al. Identification of ETV6-RUNX1-like and DUX4-rearranged subtypes in paediatric B-cell precursor acute lymphoblastic leukaemia. *Nat Commun*. 2016;7:11790.
22. Dobin A, Davis CA, Schlesinger F, et al. STAR: ultrafast universal RNA-seq aligner. *Bioinformatics*. 2013;29(1):15-21.
23. van de Geijn B, McVicker G, Gilad Y, Pritchard JK. WASP: allele-specific software for robust molecular quantitative trait locus discovery. *Nat Methods*. 2015;12(11):1061-1063.
24. Li B, Dewey CN. RSEM: accurate transcript quantification from RNA-Seq data with or without a reference genome. *BMC Bioinformatics*. 2011;12:323.
25. McCarthy S, Das S, Kretzschmar W, et al; Haplotype Reference Consortium. A reference panel of 64,976 haplotypes for genotype imputation. *Nat Genet*. 2016;48(10):1279-1283.
26. Okuyama K, Strid T, Kuruvilla J, et al. PAX5 is part of a functional transcription factor network targeted in lymphoid leukemia. *PLoS Genet*. 2019;15(8):e1008280.
27. Li H, Durbin R. Fast and accurate short read alignment with Burrows-Wheeler transform. *Bioinformatics*. 2009;25(14):1754-1760.
28. Ramírez F, Dündar F, Diehl S, Grüning BA, Manke T. deepTools: a flexible platform for exploring deep-sequencing data. *Nucleic Acids Res*. 2014;42(Web Server issue):W187-W191.
29. van Heeringen SJ, Veenstra GJ. GimmeMotifs: a de novo motif prediction pipeline for ChIP-sequencing experiments. *Bioinformatics*. 2011;27(2):270-271.
30. Weirauch MT, Yang A, Albu M, et al. Determination and inference of eukaryotic transcription factor sequence specificity. *Cell*. 2014;158(6):1431-1443.
31. Heinz S, Benner C, Spann N, et al. Simple combinations of lineage-determining transcription factors prime cis-regulatory elements required for macrophage and B cell identities. *Mol Cell*. 2010;38(4):576-589.
32. Fornes O, Castro-Mondragon JA, Khan A, et al. JASPAR 2020: update of the open-access database of transcription factor binding profiles. *Nucleic Acids Res*. 2020;48(D1):D87-D92.
33. Durand NC, Shamim MS, Machol I, et al. Juicer provides a one-click system for analyzing loop-resolution Hi-C experiments. *Cell Syst*. 2016;3(1):95-98.
34. Wu HJ, Michor F. A computational strategy to adjust for copy number in tumor Hi-C data. *Bioinformatics*. 2016;32(24):3695-3701.
35. Stansfield JC, Cresswell KG, Dozmorov MG. multiHiCcompare: joint normalization and comparative analysis of complex Hi-C experiments. *Bioinformatics*. 2019;35(17):2916-2923.
36. Crane E, Bian Q, McCord RP, et al. Condensin-driven remodelling of X chromosome topology during dosage compensation. *Nature*. 2015;523(7559):240-244.
37. Wolf J, Passmore LA. mRNA deadenylation by Pan2-Pan3. *Biochem Soc Trans*. 2014;42(1):184-187.
38. Weischenfeldt J, Dubash T, Drainas AP, et al. Pan-cancer analysis of somatic copy-number alterations implicates IRS4 and IGF2 in enhancer hijacking. *Nat Genet*. 2017;49(1):65-74.
39. Hnisz D, Weintraub AS, Day DS, et al. Activation of proto-oncogenes by disruption of chromosome neighborhoods. *Science*. 2016;351(6280):1454-1458.
40. Ooi WF, Nargund AM, Lim KJ, et al. Integrated paired-end enhancer profiling and whole-genome sequencing reveals recurrent CCNE1 and IGF2 enhancer hijacking in primary gastric adenocarcinoma. *Gut*. 2020;69(6):1039-1052.
41. Stam RW, den Boer ML, Schneider P, et al. Targeting FLT3 in primary MLL-gene-rearranged infant acute lymphoblastic leukemia. *Blood*. 2005;106(7):2484-2490.
42. Ozeki K, Kiyoi H, Hirose Y, et al. Biologic and clinical significance of the FLT3 transcript level in acute myeloid leukemia. *Blood*. 2004;103(5):1901-1908.
43. Kang H, Wilson CS, Harvey RC, et al. Gene expression profiles predictive of outcome and

age in infant acute lymphoblastic leukemia: a Children's Oncology Group study. *Blood*. 2012;119(8):1872-1881.

44. Garza-Veloz I, Martinez-Fierro ML, Jaime-Perez JC, et al. Identification of differentially expressed genes associated with prognosis of B acute lymphoblastic leukemia. *Dis Markers*. 2015;2015:828145.

45. Kuchenbauer F, Kern W, Schoch C, et al. Detailed analysis of FLT3 expression levels in acute myeloid leukemia. *Haematologica*. 2005;90(12):1617-1625.

46. Paulsson K, Horvat A, Strömbeck B, et al. Mutations of FLT3, NRAS, KRAS, and PTPN11 are frequent and possibly mutually exclusive in high hyperdiploid childhood acute lymphoblastic leukemia. *Genes Chromosomes Cancer*. 2008;47(1):26-33.

47. Li Y, Schwab C, Ryan S, et al. Constitutional and somatic rearrangement of chromosome 21 in acute lymphoblastic leukaemia. *Nature*. 2014;508(7494):98-102.

48. Yamamoto JF, Goodman MT. Patterns of leukemia incidence in the United States by subtype and demographic characteristics, 1997-2002. *Cancer Causes Control*. 2008; 19(4):379-390.

49. Paulsson K, Johansson B. High hyperdiploid childhood acute lymphoblastic leukemia. *Genes Chromosomes Cancer*. 2009;48(8):637-660.